



# Tropical forcing and ENSO dominate Holocene climates in South Africa's southern Cape

Brian M Chase, Arnoud Boom, Andrew S Carr, Paula J Reimer

## ► To cite this version:

Brian M Chase, Arnoud Boom, Andrew S Carr, Paula J Reimer. Tropical forcing and ENSO dominate Holocene climates in South Africa's southern Cape. Quaternary Science Reviews, 2024, 330, pp.108563. 10.1016/j.quascirev.2024.108563 . hal-04524323

HAL Id: hal-04524323

<https://hal.science/hal-04524323>

Submitted on 28 Mar 2024

**HAL** is a multi-disciplinary open access archive for the deposit and dissemination of scientific research documents, whether they are published or not. The documents may come from teaching and research institutions in France or abroad, or from public or private research centers.

L'archive ouverte pluridisciplinaire **HAL**, est destinée au dépôt et à la diffusion de documents scientifiques de niveau recherche, publiés ou non, émanant des établissements d'enseignement et de recherche français ou étrangers, des laboratoires publics ou privés.



# Tropical forcing and ENSO dominate Holocene climates in South Africa's southern Cape



Brian M. Chase <sup>a,b,\*</sup>, Arnoud Boom <sup>c</sup>, Andrew S. Carr <sup>c</sup>, Paula J. Reimer <sup>d</sup>

<sup>a</sup> Institut des Sciences de l'Evolution-Montpellier (ISEM), University of Montpellier, Centre National de la Recherche Scientifique (CNRS), EPHE, IRD, Montpellier, France

<sup>b</sup> Department of Environmental and Geographical Science, University of Cape Town, South Lane, Upper Campus, 7701, Rondebosch, South Africa

<sup>c</sup> School of Geography, Geology and the Environment, University of Leicester, Leicester, LE1 7RH, UK

<sup>d</sup> School of Natural and Built Environment, Geography, Archaeology and Palaeoecology, Queen's University Belfast, Belfast, BT7 1NN, Northern Ireland, UK

## ARTICLE INFO

Handling Editor: Dr Mira Matthews

**Keywords:**

Holocene  
South Africa  
Palaeoclimate  
Climate dynamics  
ENSO  
Rock hyrax middens  
Stable isotopes

## ABSTRACT

This paper explores the Holocene climatic dynamics of South Africa's southern Cape, a region that supports a large proportion of the Greater Cape Floristic Region and contains an array of important archaeological sites. While South African climates are generally characterised by marked rainfall seasonality, the southern Cape is currently situated at the interface between tropical and temperate climate systems, resulting in a largely aseasonal rainfall regime. This regime, however, is thought to have been particularly sensitive to past changes in late Quaternary boundary conditions, meaning that variability in either tropical or temperate systems could have significant environmental impacts. Evidence of past climate change, however, remains limited.

We present a 9000-year record of hydroclimatic variability obtained from rock hyrax midden stable nitrogen records, from Papkuilsfontein, on the southern slope of the Anysberg Mountains. Resolved to an average 6-year resolution and spanning the period c. 9050 cal yr BP to 1990 CE, this is the highest resolution Holocene record from southern Africa and presents a unique opportunity for the detailed study of the primary drivers and spatial gradients of Holocene climate change in the southern Cape. The data indicate a long-term decrease in aridity across the Holocene and a pattern of variability that reveals remarkable similarities with records from the South African tropics and El Niño–Southern Oscillation proxies, highlighting the significance of tropical systems as drivers of Holocene climate change in the region. This substantially expands what has been previously considered to be the zone of tropical influence, extending from a coastal phenomenon associated with heat transport via the Agulhas Current to encompass much, if not all, of the Agulhas Plain south of the Cape Fold Mountains. These findings provide a valuable new climatic framework for contextualizing changes in ecological and archaeological records in the southern Cape, and contribute to a more comprehensive understanding of the spatio-temporal dynamics of climate systems in southern Africa.

## 1. Introduction

Southern Africa, between 15°S and 35°S, is situated at the interface between tropical low latitude and temperate mid-latitude climate regimes (Fig. 1). These regimes are determined by their dominant moisture sources and the type(s) of associated moisture-bearing systems and are often defined spatially in terms of rainfall seasonality. This has given rise to a commonly used tripartite system of summer, winter and aseasonal rainfall zones. During the late Quaternary, the extent/nature of each rainfall zone is thought to have varied according to broad changes in global boundary conditions (a wetter/more extensive summer

(winter) rainfall zone during interstadial (stadial) phases) (e.g. Chase and Meadows, 2007; Cockcroft et al., 1987; Deacon and Lancaster, 1988). This system underpins the majority of interpretation of records of past environmental variability in southern Africa, with evidence of past change being generally associated with either: 1) those oceanic and atmospheric circulation systems that determine modern rainfall seasonality at a given site, or 2) those systems that are considered to strengthened/weakened during a given period (e.g. increased influence of the southern westerlies during glacial periods (Cockcroft et al., 1987; van Zinderen Bakker, 1976)).

In recent years, the acquisition of a greater density of continuous

\* Corresponding author. Institut des Sciences de l'Evolution-Montpellier (ISEM), University of Montpellier, Centre National de la Recherche Scientifique (CNRS), EPHE, IRD, Montpellier, France.

E-mail address: [brian.chase@umontpellier.fr](mailto:brian.chase@umontpellier.fr) (B.M. Chase).

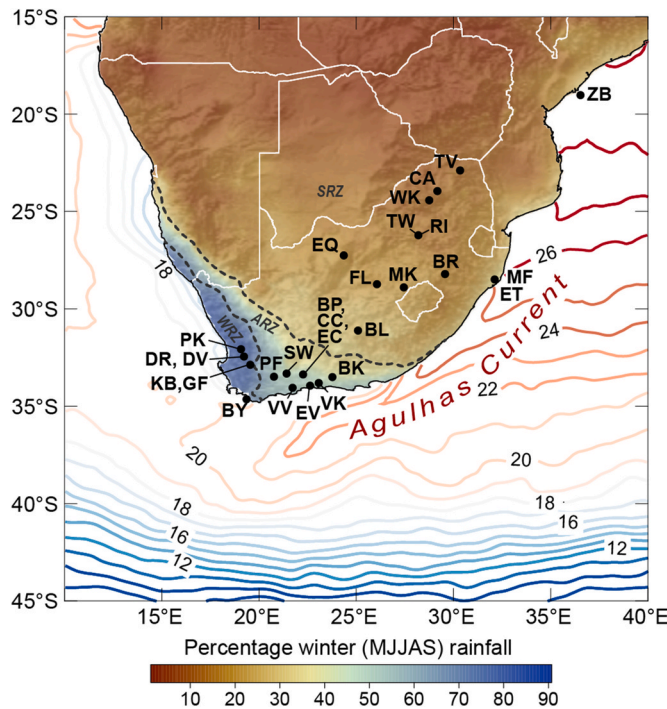


**Fig. 1.** Map of the southwestern margin of Africa showing seasonality of rainfall and sharp climatic gradients dictated by the zones of summer/tropical (red) and winter/temperate (blue) rainfall dominance. Winter, summer and aseasonal rainfall zones (WRZ, SRZ and ARZ respectively, defined according to Chase and Meadows (2007; data from Hijmans et al., 2005)), sea-surface temperatures (shown in °C; data from Reynolds et al., 2007)) and the position of the warm Agulhas Current are indicated. The location of key palaeoclimatic records discussed are shown: PK: Pakhuis Pass (Chase et al., 2019a; Scott and Woodborne, 2007a, 2007b), DR: De Rif (Chase et al., 2011, 2015a; Quick et al., 2011; Valsecchi et al., 2013), DV: Driehoek Vlei (Meadows and Sugden, 1991), KB: Katbakkies Pass (Chase et al., 2015b; Meadows et al., 2010), GF: Groenfontein (Chase et al., 2023), BY: Byneskranskop (Faith et al., 2018; Schweitzer and Wilson, 1983), VV: Voëlvlei (Strobel et al., 2021), PF: Papkuilfontein (this study), SW: Seweweekspruit (Chase et al., 2013, 2017), BP: Boomplaas Cave (Deacon et al., 1984; Faith et al., 2018), CC: Cango Caves (Chase et al., 2021; Talma and Vogel, 1992) and EC: Efflux Cave (Braun et al., 2020), EV: Eilandvlei (Quick et al., 2018; Wündsch et al., 2018), VK: Vankervelsvlei (Strobel et al., 2022), BK: Baviaanskloof (Chase et al., 2020), MK: Marakabi (Chase et al., 2022), MF: Mfabeni (Baker et al., 2014; Finch and Hill, 2008), ET: Lake Eteza (Neumann et al., 2010), CA: Cold Air Cave (Holmgren et al., 2003; Lee-Thorp et al., 2001), ZB: GeoB9307-3 marine core (Schefuß et al., 2011). Also included are the palaeoenvironmental sites used for the reconstruction (Chevalier and Chase, 2015) of southern-central summer rainfall zone climates BL: Blydefontein (Scott et al., 2005), FL: Florisbad (Scott and Nyakale, 2002), EQ: Equus Cave (Scott, 1987b) and BR: Braamhoek (Norström et al., 2009) and northern summer rainfall zone climates TW: Tswaing Crater (Metwally et al., 2014; Scott, 1999) and RI: Rietvlei (Scott and Vogel, 1983) WK: Wonderkrater (Scott, 1982) and TV: Tate Vondo (Scott, 1987a).

high resolution palaeoclimate records, largely from rock hyrax middens across southern Africa has provided broad support for these basic principles, but also highlighted a significantly more nuanced and complex picture of long-term environmental change (e.g. Chase et al., 2017). Markedly different – or even opposing – patterns of climate change have been noted within the summer (Chase et al., 2022; Chevalier and Chase, 2015; Scott et al., 2012), winter (Chase et al., 2019a) and aseasonal rainfall zones (Chase and Quick, 2018). The identification of these patterns and phenomena highlights the need for a thorough assessment of environmental change both within and between rainfall zones in order to develop a more refined understanding of the spatio-temporal dynamics of the dominant circulation systems, and to establish a more reliable interpretive framework for the region's palaeoenvironmental

records.

In this paper, we focus on South Africa's southern Cape, which encompasses the core of the aseasonal rainfall zone and is bounded by the Cape Fold Mountains to the north and the Indian Ocean to the south (Fig. 2). This region is of particular ecological and cultural significance, as it supports the major biomes that comprise the Greater Cape Floristic Region (GCFR) – Fynbos, Succulent Karoo, Albany Thicket and Afrotemperate Forest (Bergh et al., 2014), and is the home to many of South Africa's major archaeological sites, such as Die Kelders, Byneskranskop, Boomplaas Cave, Nelson Bay Cave, Blombos Cave, Pinnacle Point and Klasies River Mouth. Here, the strong seasonality characteristic of southern African climates is attenuated by the influence of winter frontal systems as well as a predominance of composite synoptic circulation systems such as cut-off lows, ridging anticyclones and tropical-temperate troughs (Engelbrecht and Landman, 2016), all of which form through interactions between tropical and temperate circulation systems (cf. tropical-temperate interactions (TTIs) as referred to by Chase et al., 2017). Southerly meridional flow, the advection of moisture off the ocean and across the coastal plain, can also bring significant rainfall to the region, enhanced as it is by orographic uplift along the southern margin of the Cape Fold mountains (Engelbrecht and Landman, 2016) and by the high latent heat flux of the Agulhas Current (Rouault et al., 2002).

The southern Cape's climatic history, however, remains poorly understood, and the context for the evolution of its vegetation and past human activity has not been adequately resolved. It has long been hypothesised that changes in rainfall source and seasonality were particularly significant, with shifts between winter and summer rainfall dominance having potentially dramatic ecological consequences (Chase and Meadows, 2007; Cowling and Lombard, 2002). Evidence for long-term environmental change has been generally limited to records recovered from coastal lakes and wetlands (Martin, 1968; Quick et al., 2015, 2016, 2018; Wündsch et al., 2018) and archaeological sites such as Boomplaas Cave (Deacon et al., 1984; Faith, 2013; Faith et al., in press; Sealy et al., 2016), Nelson Bay Cave (Faith et al., 2018; Klein, 1972; Sealy, 1996) and Byneskranskop (Faith et al., 2018; Schweitzer and Wilson, 1983). While providing important insights into environmental change at the sites, the concentration of sites along the coast and the relatively coarse resolution of the archaeological records has complicated efforts to establish a coherent picture of long-term environmental change in the southern Cape. The significance of this spatial bias has been highlighted in studies comparing records from the coastal sites, such as Eilandvlei (Quick et al., 2018; Wündsch et al., 2018), and sites from Seweweekspruit, in the Cape Fold Mountains (Chase et al., 2013, 2017). Data from these sites express generally inverse patterns of hydroclimatic change across the mid-to late Holocene, which has been suggested to reflect the influence of the Agulhas Current and the transmission of tropical climate signals to southern coastal regions (Chase and Quick, 2018). This spatio-temporal variability poses important questions regarding the extent to which “coastal” and/or “interior” climate change anomalies influence and interact to define environmental change across the core of the southern Cape and the Agulhas Plain.

Presented here is a c. 9000-year stable nitrogen isotope record obtained from rock hyrax middens collected from a site known as Papkuilfontein (Fig. 2). This site was selected for its position on the northern margin of the Agulhas Plain and its proximity to the modern junction between the winter and aseasonal rainfall zones. As a proxy for hydroclimatic variability, and considered in the context of comparable data from other regional sites, we are able to use the Papkuilfontein data to better define Holocene climate change gradients in the southern Cape and identify the likely drivers of climate change in the region.

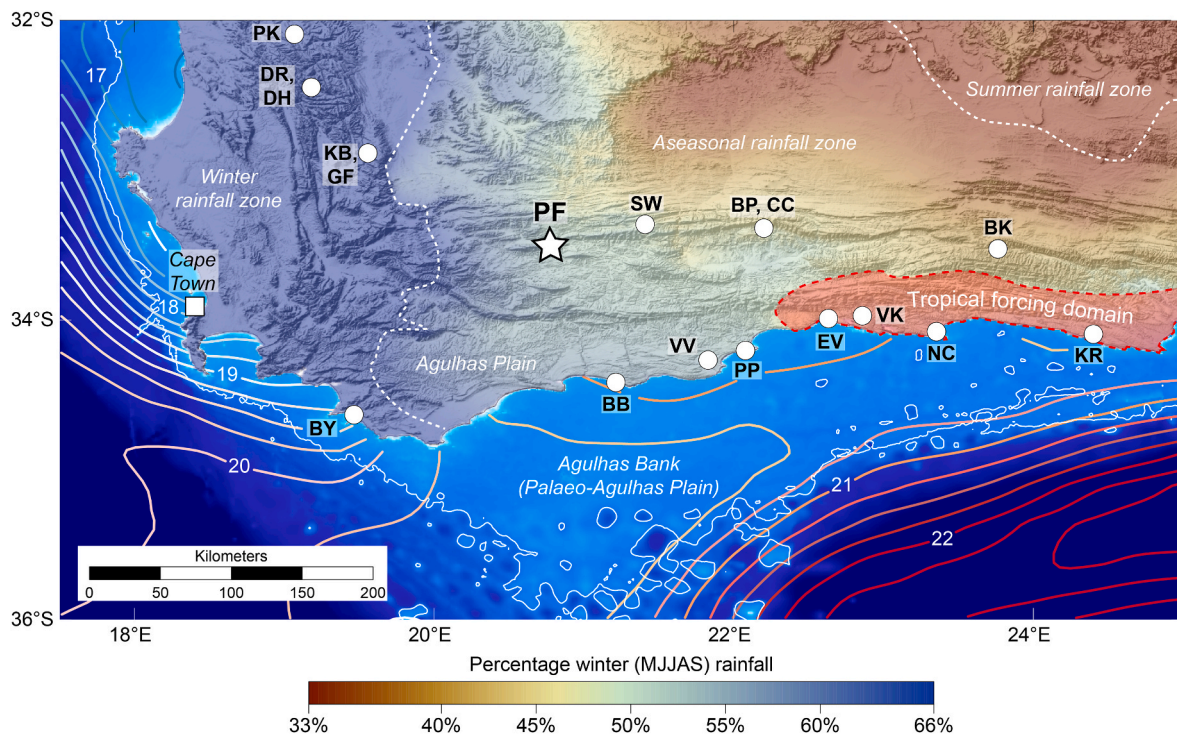


**Fig. 2.** Map of southern Cape study region. The location of the Papkuilfontein hyrax midden site (PF) is indicated, as are other key Holocene sites, including PK: Pakhuis Pass (Chase et al., 2019a; Scott and Woodborne, 2007a, 2007b), DR: De Rif (Chase et al., 2011, 2015a; Quick et al., 2011; Valsecchi et al., 2013), DH: Driehoek Vlei (Meadows and Sugden, 1991), KB: Katbakkies Pass (Chase et al., 2015b; Meadows et al., 2010), GF: Groenfontein (Chase et al., 2023), SW: Seweweekspruit (Chase et al., 2013, 2017), CC: Cango Caves (Chase et al., 2021; Talma and Vogel, 1992), VV: Voëlvlei (Strobel et al., 2021), EV: Eilandvlei (Quick et al., 2018; Wündsch et al., 2018), VK: Vankervelsvlei (Strobel et al., 2022), BK: Baviaanskloof (Chase et al., 2020) and the archaeological sites of BP: Boomplaas Cave (Deacon et al., 1984; Faith et al., 2018), BY: Byneskranskop (Faith et al., 2018; Schweitzer and Wilson, 1983), BB: Blombos Cave (Henshilwood et al., 2001), PP: Pinnacle Point (Marean, 2010), NC: Nelson Bay Cave (Deacon, 1978; Faith et al., 2018; Sealy et al., 2020) and KR: Klasies River Mouth (Deacon et al., 1986; Klein, 1975; Reynard and Wurz, 2020). Shading indicates the regional rainfall seasonality gradient defined according to Chase and Meadows (2007; data from Hijmans et al., 2005)), with winter, aseasonal and summer rainfall zones delimited by dashed white lines. The extent of the zone of near-coast Holocene tropical climate forcing proposed by Chase and Quick (2018) is indicated by the dashed red line. The digital elevation model is from Yamazaki et al. (2017), the -130 m bathymetric isoline indicating the maximum extent of the Agulhas Plain during the Last Glacial Maximum is shown as a solid white line (data from GEBCO, 2012) and isolines indicating mean January sea-surfaces temperatures (1982–2010) at 0.25 °C intervals (data from Reynolds et al., 2007).

## 2. Site description, material and methods

### 2.1. Site description

Two adjacent rock hyrax middens were collected from a cliff in the Cape Supergroup quartzites of the southern flank of the Anysberg mountains (33.504°S, 20.776°E; 625 m.a.s.l.), a subsidiary range of the east-west axis of the Cape Fold Mountains (Fig. 2). The vegetation at the

site is South Swartberg Sandstone Fynbos, a proteoid-restioid fynbos type (Rebelo et al., 2006). The slopes below the cliff bands are composed of shales, and support a Western Little Karoo vegetation dominated by asteraceous and succulent shrubs (Mucina et al., 2006). The region is characterised by a “cold semi-arid” climate (BSk Köppen-Geiger classification; Peel et al., 2007), with mean monthly temperatures ranging from 10.1 °C in July to 22.7 °C in February. Mean annual rainfall at the site is ~245 mm/yr and is generally distributed evenly across the year



**Fig. 3.** (A) The Papkuilfontein-1-1 rock hyrax midden, (B) sampling the Papkuilfontein-1-3 midden, and (C) the Papkuilfontein-1-1 midden with sections 1-1a and 1-1b removed (1-1b seen laying next to remaining midden).

(data from [Hijmans et al., 2005](#)).

## 2.2. Midden collection

The selection of middens and the methods employed to analyse them follow the procedures described elsewhere by [Chase et al. \(2020, 2019b, 2012\)](#). The Papkuilfontein-1 middens – PKF-1-1 and PKF-1-3 – were found within close proximity of each other (~10 m) ([Fig. 3](#)) and were selected for their thickness and high hyraceum (crystallised urine) content. Proxies obtained from hyraceum are considered to represent environmental conditions more clearly than samples containing high proportions of faecal pellets, which may 1) include a degree of dietary bias, 2) lack the stratigraphic integrity of hyraceum-rich middens, and 3) are poor temporal integrators, reflecting the discrete periods during which the animals are consuming the food that is excreted ([Carr et al., 2016; Chase et al., 2012](#)). Representative sections of each midden ([Fig. 3](#)) were cut perpendicular to the stratigraphy using an angle grinder and transported back to the laboratory where each section was cleaned using progressively finer grades of sandpaper prior to sampling. During collection, PKF-1-1 was collected as two abutting sections, labelled 1-1a and 1-1b. The PKF-1-3 midden formed with a sloping aspect due to the angle of the ledge upon which it accumulated. To maximise the potential of the midden, samples were taken from three overlapping transects, for which three separate age models were calculated ([Fig. 4](#)).

## 2.3. Chronology

Radiocarbon age determinations for the PKF-1-1 and PKF-1-3

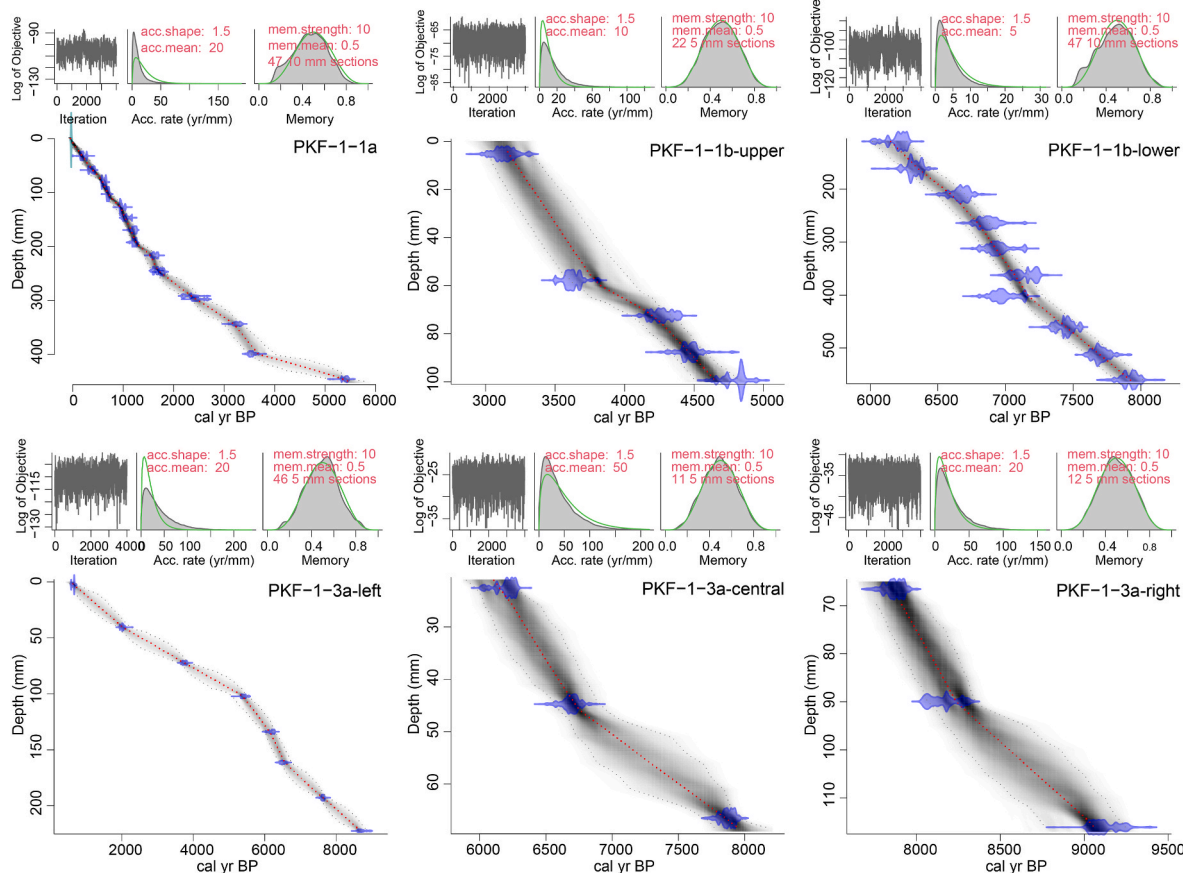


**Fig. 4.** Distribution in time and depth of  $^{14}\text{C}$  ages for the Papkuilfontein (PKF)-1 rock hyrax midden with age-depth model (grey), overlaying the calibrated distributions of the individual dates calculated using the R package Bacon v2.5.8 ([Blaauw and Christen, 2011](#)). Red dotted lines indicate the 'best' model based on the mean age.

middens ( $n = 46$ ) were processed at the  $^{14}\text{CHRONO}$  Centre, Queen's University Belfast using accelerator mass spectrometry (AMS) ([Table 1](#); [Fig. 4](#)). Samples were pre-treated with 2% HCl for 1 h at room temperature to remove carbonates and dried at 60 °C. They were then weighed into quartz tubes with an excess of CuO, sealed under vacuum and combusted to  $\text{CO}_2$ . The  $\text{CO}_2$  was converted to graphite on an iron catalyst using the zinc reduction method ([Slota et al., 1987](#)). The radiocarbon ages were corrected for isotope fractionation using the AMS measured  $\delta^{13}\text{C}$ . The ages were calibrated using the SHCal20 calibration data ([Hogg et al., 2020](#)). Post-bomb ages were calibrated using CALIBOMB (Reimer and Reimer, 2023) and the SHZ1\_2 post-bomb calibration dataset ([Hua et al., 2021](#)). The rbacon v.3.0.0 software package ([Blaauw and Christen, 2011; Blaauw et al., 2020](#)) was used to generate the age-depth models ([Fig. 4](#)).

## 2.4. Stable nitrogen isotopes

The stable nitrogen isotope composition of 1444 hyraceum samples (approx. 2 mg) were measured at the School of Geography, Geology and the Environment, University of Leicester. Samples were obtained from two offset tracks using a 1 mm drill, creating a quasi-continuous record of overlapping samples. Isotope ratios were measured on a Sercon 20-20 continuous flow isotope ratio mass spectrometer. For the  $^{15}\text{N}$  stable isotope analyses, the standard deviation derived from replicate analyses of homogeneous reference material (Casein protein CatNo.B2155 Batch no. 114859 Elemental Microanalysis Ltd UK) was better than 0.2‰. The results are expressed relative to atmospheric nitrogen.

**Table 1**

Radiocarbon ages and calibration information for the Papkuilfontein-1 rock hyrax middens.

Sample	Depth range (mm)	14C age yr BP	1 sigma error	calibration data	95.4 % (2σ) lower cal range BP	95.4 % (2σ) upper cal range BP	relative area under distribution	median probability (cal BP)
<b>PKF-1-1a</b>								
UBA-24433	2.89–5.15	F14C 1.2913	0.0028	SHCal13; SHZ1_2	−30.91 −30.96 −29.58 −13.33	−30.74 −29.81 −29.5 −13.2	3.7% 79.5% 1.1% 15.7%	−30
UBA-29401	33.42–34.67	228	19	SHCal20	145 265	219 287	82.8% 17.2%	193
UBA-29093	58.42–60.80	332	22	SHCal20	301 359	332 444	27.5% 72.5%	390
UBA-29402	80.40–83.29	725	23	SHCal20	565 631	596 669	46.2% 53.8%	635
UBA-29094	102.76–105.15	816	23	SHCal20	669	728	100.0%	702
UBA-24435	126.51–129.52	1105	23	SHCal20	926 1026	982 1049	84.1% 15.9%	953
UBA-24436	145.35–149.87	1201	28	SHCal20	962 1041 1134	1037 1104 1176	48.8% 32.8% 18.4%	1050
UBA-31656	168.84–171.73	1321	27	SHCal20	1105 1156 1176	1140 1163 1279	9.3% 1.0% 89.8%	1225
UBA-29095	191.58–194.60	1330	22	SHCal20	1177	1277	100.0%	1229
UBA-29405	215.58–218.84	1751	27	SHCal20	1539 1560 1643	1551 1636 1700	4.2% 52.8% 43.0%	1619
UBA-29096	245.98–248.87	1758	21	SHCal20	1565 1642	1639 1700	49.0% 51.0%	1639
UBA-29406	243.72–247.23	1872	22	SHCal20	1705 1762	1756 1826	43.2% 56.8%	1773
UBA-21367	290.32–293.84	2360	41	SHCal20	2147 2297 2480	2264 2466 2487	46.1% 53.2% 0.7%	2316
UBA-29097	296.60–299.49	2457	24	SHCal20	2349 2530 2565 2586 2635	2519 2537 2567 2615 2699	75.2% 0.6% 0.3% 7.2% 16.8%	2454
UBA-29098	342.33–345.10	3084	31	SHCal20	3084 3150	3088 3364	0.3% 99.7%	3254
UBA-29099	397.11–400.87	3356	29	SHCal20	3454 3479 3599 3670	3475 3594 3636 3680	6.9% 83.5% 8.1% 1.5%	3532
UBA-21368	443.59–447.36	4677	28	SHCal20	5309	5466	100.0%	5404
<b>PKF-1-1b upper section</b>								
UBA-20651	3.99–6.55	3007	30	SHCal20	3000 3303	3246 3321	97.7% 2.3%	3136
UBA-29407	55.91–59.58	3417	25	SHCal20	3493 3559 3707 3806	3523 3700 3715 3811	6.1% 92.9% 0.6% 0.4%	3617
UBA-30360	71.09–73.80	3886	24	SHCal20	4153 4217	4211 4406	24.2% 75.8%	4269
UBA-30361	86.26–88.98	4031	31	SHCal20	4299 4353 4400	4327 4371 4574	2.2% 1.5% 96.3%	4473
UBA-30362	97.92–100.80	4293	27	SHCal20	4648 4698 4802 4943	4674 4757 4874 4952	4.8% 20.3% 74.3% 0.6%	4837
<b>PKF-1-1b lower section</b>								
UBA-29408	108.31–111.50	5440	28	SHCal20	6013 6064 6114 6175	6045 6073 6146 6293	4.9% 0.9% 10.7% 83.5%	6224
UBA-29409	159.74–162.78	5557	32	SHCal20	6217 6276	6234 6398	4.1% 95.9%	6321
UBA-29410	208.31–211.50	5892	30	SHCal20	6558 6764	6750 6781	97.6% 2.4%	6677
UBA-29411	261.18–266.77	6061	38	SHCal20	6746	6982	100.0%	6867

(continued on next page)

**Table 1** (continued)

Sample	Depth range (mm)	14C age yr BP	1 sigma error	calibration data	95.4 % (2σ) lower cal range BP	95.4 % (2σ) upper cal range BP	relative area under distribution	median probability (cal BP)
UBA-29412	310.70–313.58	6111	33	SHCal20	6793 7054 7121	7020 7058 7155	93.0% 0.2% 6.8%	6931
UBA-29413	360.70–363.90	6276	30	SHCal20	7010 7152	7129 7257	44.8% 55.2%	7162
UBA-29414	400.16–403.83	6139	31	SHCal20	6854 7099	7078 7157	82.8% 17.2%	6973
UBA-29415	458.63–461.98	6568	35	SHCal20	7329 7416 7539	7394 7512 7562	22.8% 70.5% 6.7%	7450
UBA-29416	510.86–514.22	6897	35	SHCal20	7606	7790	100.0%	7692
UBA-30363	558.31–561.82	7139	43	SHCal20	7800 7836	7805 8015	0.7% 99.3%	7931
<b>PKF-1-3a left track</b>								
UBA-30364	0.96–3.99	750	20	SHCal20	568 637	590 677	26.2% 73.8%	660
UBA-30365	38.48–42.33	2091	23	SHCal20	1930 1990 2068	1969 2062 2088	26.1% 66.3% 7.6%	2012
UBA-30366	70.77–73.80	3500	23	SHCal20	3641 3682	3669 3833	12.3% 87.7%	3744
UBA-30367	100.73–103.76	4723	27	SHCal20	5318 5534	5479 5567	94.1% 5.9%	5398
UBA-30368	132.34–135.36	5431	31	SHCal20	6008 6058 6112 6172	6050 6078 6149 6291	8.3% 3.0% 13.9% 74.8%	6212
UBA-30369	159.83–162.85	5747	29	SHCal20	6403 6581	6569 6626	89.2% 10.8%	6497
UBA-30370	191.16–194.46	6813	31	SHCal20	7574	7678	100.0%	7627
UBA-30371	220.29–224.55	7920	32	SHCal20	8553 8588 8828 8880 8914	8567 8785 8865 8896 8980	0.9% 83.3% 6.1% 1.5% 8.1%	8691
<b>PKF-1-3a central track</b>								
UBA-30372	21.03–24.05	5439	28	SHCal20	6013 6064 6114 6175	6046 6073 6147 6293	5.1% 1.0% 10.9% 82.9%	6223
UBA-30373	42.74–46.72	5907	32	SHCal20	6563 6604	6587 6789	3.7% 96.3%	6295
UBA-30374	64.86–68.16	7077	29	SHCal20	7787	7958	100.0%	7875
<b>PKF-1-3a right track</b>								
UBA-30374	64.86–68.16	7077	29	SHCal20	7787	7958	100.0%	7875
UBA-30375	88.36–91.53	7400	29	SHCal20	8031 8249	8217 8318	80.4% 19.6%	8165
UBA-30376	114.20–118.05	8199	31	SHCal20	9008 9171	9146 9268	75.6% 24.4%	9099

### 3. Results and interpretive basis

#### 3.1. Chronology

Radiocarbon analyses indicate that the Papkuilfontein-1 hyrax middens accumulated between c. 1990 CE to 9060 cal yr BP (Table 1; Fig. 4). The age-depth models for the Papkuilfontein-1 middens suggests continuous deposition, with the possible exception of the PKF-1b section, which exhibits a marked decline in accumulation rates beginning between 6290 and 4830 cal yr BP (100–109 mm depth), decreasing from ~1 mm/3.5 years to ~1 mm/19.4 years. To adequately account for this rapid change, age models have been calculated separately for the upper and lower sections (Fig. 4). Overall, on average, each overlapping 1 mm sample is estimated to integrate 6.3 years of urine deposition.

#### 3.2. Stable nitrogen and their interpretation

The stable isotope samples from the Papkuilfontein midden sections were combined and sorted according to age as estimated by the age model for each section. Considered together, the  $\delta^{15}\text{N}$  values from the Papkuilfontein middens vary from 6.7 to 18.6‰ (Fig. 5), with modern midden  $\delta^{15}\text{N}$  (Fig. 5) closely matching contemporary hyrax feeding habits (modern hyrax faecal  $\delta^{15}\text{N}$  is  $7.8 \pm 2\text{‰}$ ). The highest  $\delta^{15}\text{N}$  values – and highest consistent variance in the record – occur during the early to early-mid-Holocene, with particularly high  $\delta^{15}\text{N}$  values during the period from 7300 to 6400 cal yr BP. The highest consistent variance in the record is also evident prior to 6400 cal yr BP. Following this phase, there is a stepwise decrease in  $\delta^{15}\text{N}$  values across the Holocene, with change point detection (abrupt changes in the mean; Killick et al., 2012) indicating shifts at 6410, 3210, 1150 and 360 cal yr BP (Fig. 5). Continuous Morlet wavelet transform analysis indicates significant variability at ~4000–3600, ~2600–2500, ~1800–1400 and

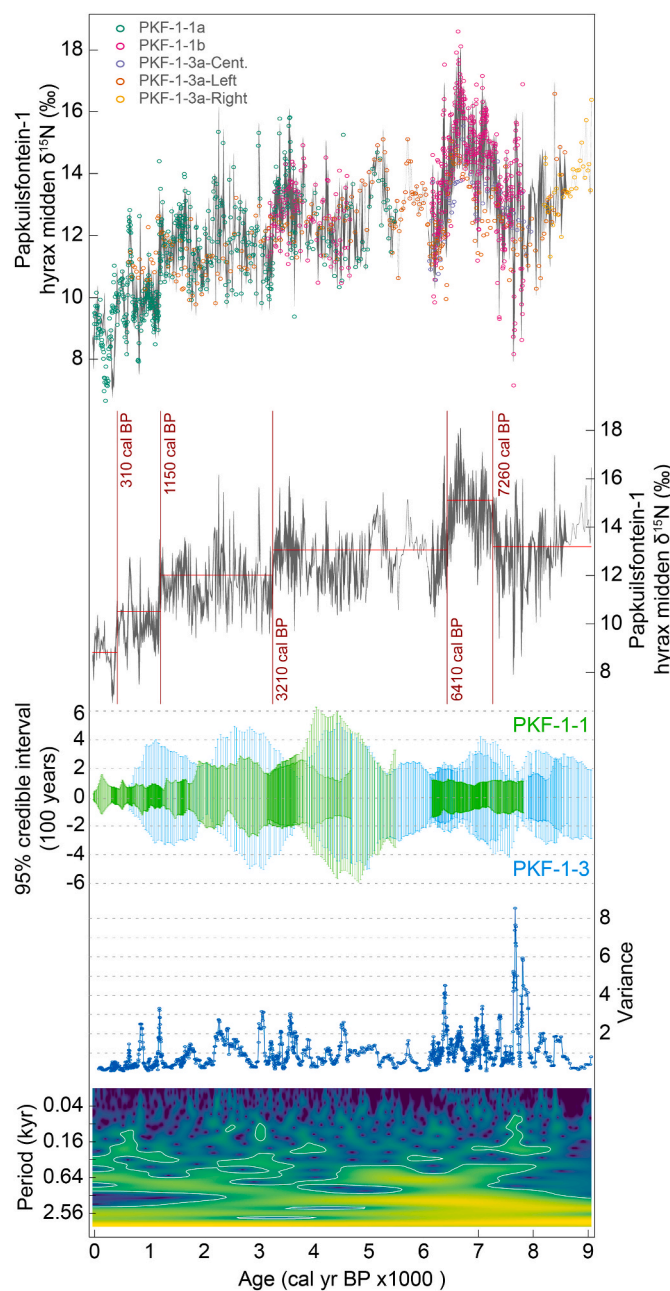


**Fig. 5.** The  $\delta^{15}\text{N}$  data from the Papkuilfontein-1 rock hyrax middens. (A) The data points from each midden section included in the composite  $\delta^{15}\text{N}$  record are shown overlaying the composite result (in grey) derived using Gaussian kernel smoothing of the age-ranked data (Rehfeld et al., 2011). (B) Results of change point analysis indicating most significant changes in mean values in the composite  $\delta^{15}\text{N}$  record are shown in red. (C) 95% credible interval associated with the age-depth model for each sample from each midden are indicated. (D) The variance of the record was calculated over time using the R package Zoo (Zeileis and Grothendieck, 2005) with a 10-point moving window. Lower pane (E) shows local Morlet wavelet power spectrum for the composite  $\delta^{15}\text{N}$  record, with white line delimiting greater than 95% confidence using a white-noise model (Hammer et al., 2001).

~950–650-year periodicities. The strength of these signals is variable across the Holocene, with the ~1800–1400-year cycle being most prevalent between 9000 and 2500 cal yr BP, before declining in the last two millennia, and the ~950–650-year cycle being most significant during two phases, between ~7000 and 4500 cal yr BP and during the last 2000 years (Fig. 5).

Variations in midden  $\delta^{15}\text{N}$  are interpreted (as per other studies of

nitrogen isotopes in hyraxes, e.g. Chase et al., 2019a; Chase et al., 2009; Chase et al., 2019b; Chase et al., 2012) to reflect changes in aridity. This is generally attributed to a more open nitrogen cycle in arid regions. In more humid regions, N is cycled between live and dead organic pools, while in drier regions more N flows to mineral pools where it is subject to gaseous loss of lighter  $^{14}\text{N}$  (Austin and Vitousek, 1998). The  $\delta^{15}\text{N}$  value of soils is thus higher with increasing aridity (Handley et al., 1999; Murphy and Bowman, 2009). The relationship recognised between aridity and soil  $^{15}\text{N}$  is transmitted to, and replicated in, plant and animal tissues, including herbivore faecal matter (e.g. Aranibar et al., 2008; Carr et al., 2016; Craine et al., 2009; Hartman, 2011; Hartman and Danin, 2010; Murphy and Bowman, 2006; Newsome et al., 2011; Swap et al., 2004). Studies of  $^{15}\text{N}$  in hyrax middens from a wide range of environments indicate consistently strong correlations between midden  $^{15}\text{N}$  and independent climate proxy records, supporting the conclusion that aridity is a major driver of midden  $^{15}\text{N}$  records (Carr et al., 2016; Chase et al., 2009, 2015a, 2017, 2019b).

#### 4. Discussion

The Papkuilfontein-1  $\delta^{15}\text{N}$  is the most highly resolved Holocene palaeoclimate record yet recovered from southern Africa (cf. Holmgren et al., 2003). On average, each overlapping 1 mm sample integrates 6.3 years of urine deposition, resulting in an interval-free record capable of characterising variations in hydroclimate at multi-decadal to multi-millennial timescales.

Conditions at the site appear to have been driest (higher  $\delta^{15}\text{N}$  values) during the early-to-early mid-Holocene, with a general trend towards increased humidity from the mid to late Holocene. The observed long-term trend from relative aridity to relative humidity across the Holocene is broadly consistent with increasing summer insolation (Fig. 6); a pattern predicted (Chase, 2021; Partridge et al., 1997) and observed at sites in the northern summer rainfall zone (Chevalier and Chase, 2015; Holmgren et al., 2003; Metwally et al., 2014; Scott, 1982; Scott et al., 2005). Its prevalence at a site in such close proximity to the winter rainfall zone, where records from sites such as Driehoek Vlei (Meadows and Sugden, 1991), De Rif (Chase et al., 2015a), Pakhuis Pass (Chase et al., 2019a; Scott and Woodborne, 2007b), Katbakkies Pass (Chase et al., 2015b) and Groenfontein (Chase et al., 2023) do not indicate a clear signal of direct insolation forcing during the Holocene (Figs. 1 and 7) is particularly interesting.

Most interestingly, marked parallels are also evident between the Papkuilfontein record and sites from the summer rainfall zone at millennial timescales, with particularly striking similarities existing with the Cold Air Cave speleothem  $\delta^{13}\text{C}$  record (Holmgren et al., 2003) and the Marakabi hyrax midden  $\delta^{15}\text{N}$  record (Chase et al., 2022)(Fig. 6). During the early and mid-Holocene, each of these records exhibits a clear, shared pattern of variability at ~1800–1400-year frequencies that have been associated with the influence of tropical systems in the South African summer and aseasonal rainfall zones (Chase et al., 2020, 2022; Chase and Quick, 2018) (Fig. 8).

Comparisons with proxies for El Niño Southern Oscillation (ENSO), such as lithic concentrations and fluxes in marine core SO147-106 KL from off the coast of Peru (Rein et al., 2005), suggest very strong relationships between ENSO variability and Holocene climates in the southern Cape, suggesting a driver for the millennial-scale patterns observed (Fig. 6). In general terms, El Niño events have been linked to reduced precipitation in the southern Cape (Engelbrecht and Landman, 2016) and summer rainfall zone (Landman and Beraki, 2012; Nicholson and Kim, 1997; Reason et al., 2000) through the position of the Walker circulation over the eastern continental margin and the reduced frequency of composite synoptic systems such as tropical-temperate troughs (Hart et al., 2018; Tozuka et al., 2014) and cut-off lows (Weldon and Reason, 2014).

It has been indicated that ENSO has been an important driver of climate change in southern Africa in recent centuries based on historical

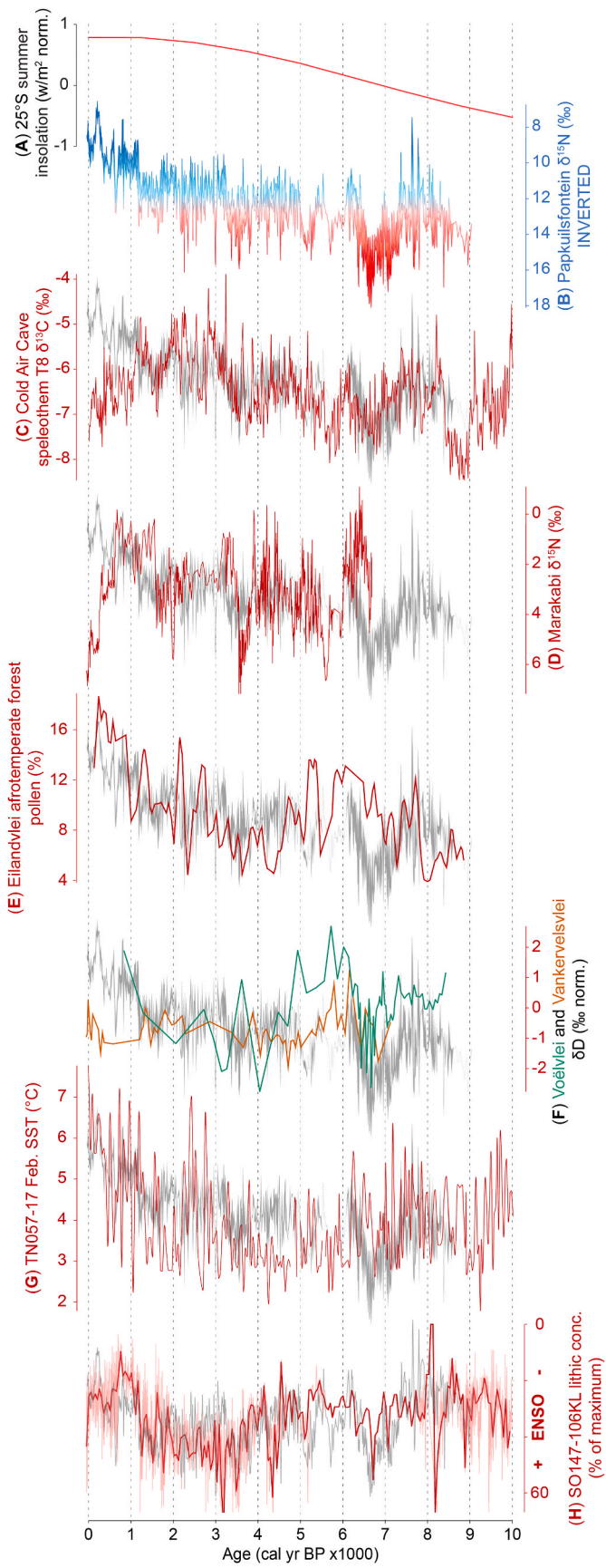


**Fig. 6.** Comparison of Papkuilfontein  $\delta^{15}\text{N}$  record (B) with drivers and regional records associated with tropical climate systems and conditions in the southern Cape, including (A) summer insolation at 25°S (Laskar et al., 2004), (C) the Cold Air Cave speleothem T8  $\delta^{13}\text{C}$  record (Holmgren et al., 2003), (D) the Marakabi-1 rock hyrax midden  $\delta^{15}\text{N}$  record (Chase et al., 2022; Chase and Meadows, 2007), (E) the Eilandvlei afrotemperate pollen record (Chase and Meadows, 2007; Deacon and Lancaster, 1988; Quick et al., 2018), (F)  $\delta\text{D}$   $n$ -alkane records from Vankervelsvlei (Strobel et al., 2022) and Voëlvlei (Strobel et al., 2021), normalised using a standard score (G) the February sea-surface temperature record from marine core TN057-17 in the African sector of the Southern Ocean (Nielsen et al., 2004) and (H) the lithic concentration record from marine core SO147-106 KL, an ENSO proxy record from the Peruvian coastal margin (Rein et al., 2005), smoothed using a Gaussian kernel method (Rehfeld et al., 2011). For clarity, the Papkuilfontein  $\delta^{15}\text{N}$  record is shown in grey with each compared proxy record. In pane H, the Papkuilfontein  $\delta^{15}\text{N}$  record has been detrended to highlight the relevant millennial-scale oscillations.

records (David, 2017) and high resolution coral  $\delta^{18}\text{O}$  records (Zinke et al., 2004). In the southern Cape, over longer time scales, the significance of ENSO has also been suggested based on lower resolution data from coastal sites (e.g. Strobel et al., 2024), but the resolution and location of the Papkuilfontein record more clearly defines the strength of the relationship and the geographic extent of the signal in the region, extending across the Agulhas Plain.

The strong correlation between the Papkuilfontein  $\delta^{15}\text{N}$  and Cold Air Cave  $\delta^{13}\text{C}$  records ends abruptly at ~1300 cal yr BP, with conditions at Papkuilfontein shifting to a phase of increased humidity, while conditions at Cold Air Cave become markedly drier (Figs. 6 and 8). This phase of late Holocene humidity is also evident in the Eilandvlei records (Fig. 6; Quick et al., 2018; Wündsch et al., 2018), suggesting - in the absence of a similar signal in the northern summer rainfall zone - factors that may be regionally specific to the southern Cape begin to dominate after 1300 cal yr BP. Consistent with the timing of this trend, sea-surface temperatures in the African sector of the Southern Ocean (site TN057-17; 50°S, 6°E) experience a mean increase at ~1300 cal yr BP (Fig. 6) at the same time that sea-ice presence indicators decline dramatically (Nielsen et al., 2004) (Fig. 7). Considering the role that changes in regional sea-surface temperatures have at some Cape coastal sites (Quick et al., 2021), we suggest that these changes in the Southern Ocean may have influenced regional climates, increasing the potential for evaporation and moisture advection across the southern Cape coastal plain.

The Papkuilfontein record provides important evidence for the spatial extent of climate change anomalies. Chase and Quick (2018) highlighted an apparent antiphase pattern of Holocene climate change between coastal sites, such as Eilandvlei (Fig. 6; Quick et al., 2018; Wündsch et al., 2018) and sites from the northern slope of the Cape Fold Mountains and the interior such as Seweweekspoort (Chase et al., 2017) and south-central summer rainfall zone composite reconstructions (Chevalier and Chase, 2015). Chase and Quick (2018) identified a strong similarity between patterns of climate change at coastal sites and conditions in the northern summer rainfall zone, indicating the dominant influence of tropical climate drivers along the southern Cape coast, likely transmitted via the Agulhas Current and associated sea-surface temperature variability. More coarsely resolved water isotope records from the near-coastal sites at Vankervelsvlei (Strobel et al., 2022) and Voëlvlei (Strobel et al., 2021) may support this basic premise - that increased tropical influence during the Holocene results in more humid conditions - although the various influences on these isotopic signals (Dansgaard, 1964; Harris et al., 2010) remain to be fully resolved in this complex region (Chase et al., 2021).

The Papkuilfontein data, and its strong similarities with the coastal and tropical records, suggests that the influence of tropical systems during the Holocene has not been limited to the coast, but extends across much of the Agulhas Plain up to the foothills of the Cape Fold Mountains

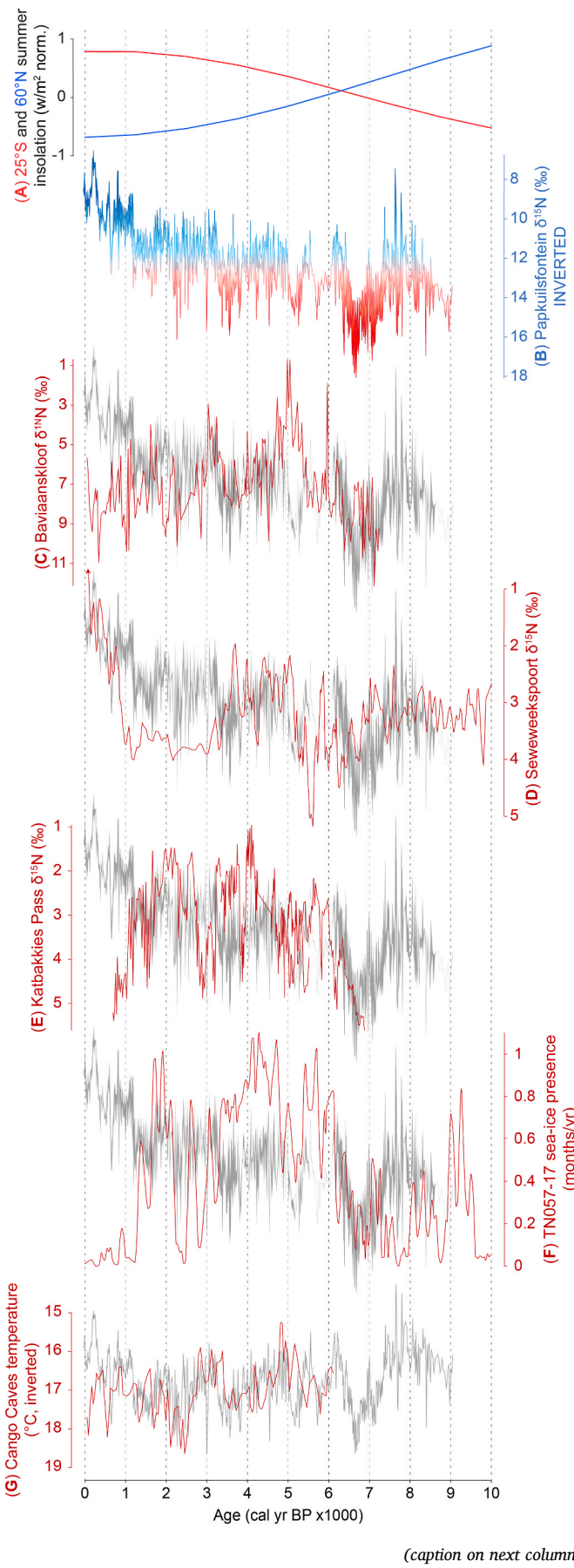


**Fig. 7.** Comparison of Papkuilsfontein  $\delta^{15}\text{N}$  record (B) with drivers and regional records associated with temperate climate systems (A) including summer insolation at 25°S and 60°N (Laskar et al., 2004), (C) the Baviaanskloof  $\delta^{15}\text{N}$  record (Chase et al., 2020), (D) the Seweweekspoort  $\delta^{15}\text{N}$  record, (E) the Katbakkies Pass  $\delta^{15}\text{N}$  record (Chase et al., 2015b), (F) the sea-ice presence record from the marine core TN057-17 in the African sector of the Southern Ocean (Nielsen et al., 2004), and (G) the palaeotemperature record from speleothems from the Cango Caves (Talma and Vogel, 1992). In pane G, the Papkuilsfontein  $\delta^{15}\text{N}$  record has been detrended to highlight the relevant millennial-scale oscillations.

(Fig. 9). Comparisons with sites from within the Cape Fold Mountains (e.g. Baviaanskloof; Chase et al., 2020; Fig. 7), express a sufficient degree of dissimilarity with the Papkuilsfontein record as to suggest that the zone of strong tropical influence during the Holocene may have been largely restricted to the coastal plain, with other factors, including orographic effects, becoming increasingly significant to the north. In comparison, temperature variability, being more spatially homogenous, does appear to have a degree of influence over aridity at Papkuilsfontein, with cooler periods recorded in the Cango Cave speleothem record (Talma and Vogel, 1992) corresponding with phases of increased humidity at Papkuilsfontein (Fig. 7).

These findings enable a significant refinement of our understanding of climate response regions in southern Africa. Recent studies have indicated that traditional models based on winter, summer and aseasonal rainfall zones (e.g. Chase and Meadows, 2007; Cockcroft et al., 1987; Deacon and Lancaster, 1988) do not adequately encapsulate the spatial variability of climate change anomalies, with significant differences being observed in records from each rainfall zone (Chase et al., 2019a; Chase and Quick, 2018; Chevalier and Chase, 2015). As such, the identification of regions that have experienced similar climate histories enables the appropriate extrapolation of palaeoenvironmental records across space, allowing for more reliable associations and comparisons to be made between sites.

This is of particular importance in the southern Cape, which hosts many archaeological sites that have provided information regarding the history and evolution of anatomically modern humans. While the Papkuilsfontein record only spans the Holocene, results are similar to rainfall seasonality and palaeo-aridity reconstructions for this period based on micromammal assemblages from Boomplaas Cave and Byneskranskop 1 (Fig. 10; Faith et al., 2018), and the general pattern of  $\delta^{15}\text{N}$  variability in the bones of grazing animals recovered from Nelson Bay Cave (Sealy, 1996). The resolution of the archaeological sequences are extremely coarse relative to the Papkuilsfontein record, and their chronologies remain to be fully resolved (Loftus et al., 2016; Pargeter et al., 2018) but the Byneskranskop and Boomplaas reconstructions both indicate an increase in summer rain across the Holocene (Fig. 10). At Byneskranskop, conditions appear to have been more arid during the early mid-Holocene during the most arid periods recorded at Papkuilsfontein. At Boomplaas, variability in both rainfall seasonality and aridity seems to be relatively muted, but it is unclear whether this is a result of the site's position further from the coast, or an effect of averaging extended periods of time in each sample. Explicit consideration of potential relationships between climate and material culture are beyond the scope of this paper, but records such as that recovered from Papkuilsfontein are now providing high-resolution climatic frameworks capable of more accurately contextualizing changes in regional archaeological records.

## 5. Conclusions

The stable nitrogen isotope data from the Papkuilsfontein rock hyrax middens has provided a highly-resolved record of climate change in the southern Cape spanning the last 9000 years. While past research has predominantly focused on coastal sites and relatively coarse archaeological records, the findings presented in this study address longstanding

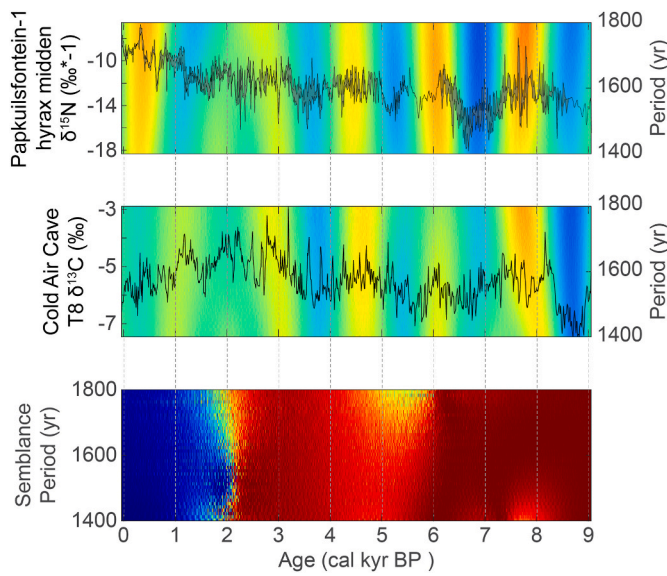


**Fig. 8.** The Papkuilfontein  $\delta^{15}\text{N}$  record (A) and (B) the  $\delta^{13}\text{C}$  record from Cold Air Cave (Holmgren et al., 2003), and (C) the results of semblance analysis (Cooper and Cowan, 2008) for the dominant 1750-yr frequency of these records, wherein red indicates a semblance of +1 (positive correlation), and blue indicates a semblance of -1 (negative correlation).

gaps in knowledge regarding the spatio-temporal evolution of climate change signals across the southern Cape and Agulhas Plain.

The Papkuilfontein  $\delta^{15}\text{N}$  record exhibits remarkable similarities with tropical records such as the  $\delta^{13}\text{C}$  record from Cold Air Cave (Holmgren et al., 2003) in South Africa's northern summer rainfall zone, suggesting that the transmission of tropical climate signals were not just limited to the coastal margin (cf. Chase and Quick, 2018), but likely extended across much of the Agulhas Plain. Comparison with proxy data reflecting ENSO variability (Rein et al., 2005) indicates a strong link between ENSO and Holocene climate change in the southern Cape. However, the abrupt divergence between Papkuilfontein and Cold Air Cave records around 1300 cal yr BP suggests a shift in regional climate dynamics. The observed late Holocene humidity in the southern Cape, concurrent with changes in Southern Ocean sea-surface temperatures, introduces the notion of regionally specific influences modulating or superseding remote tropical drivers under certain conditions. This research challenges traditional models based on rainfall zones, highlighting the inadequacy of such classifications in capturing the spatial variability of climate change anomalies. By identifying regions with similar climate histories, the study opens avenues for more reliable comparisons and associations between palaeoenvironmental records, crucial for our understanding of past environments in the southern Cape and their intersections with human societies.

#### Data availability

Data will be made available on request.

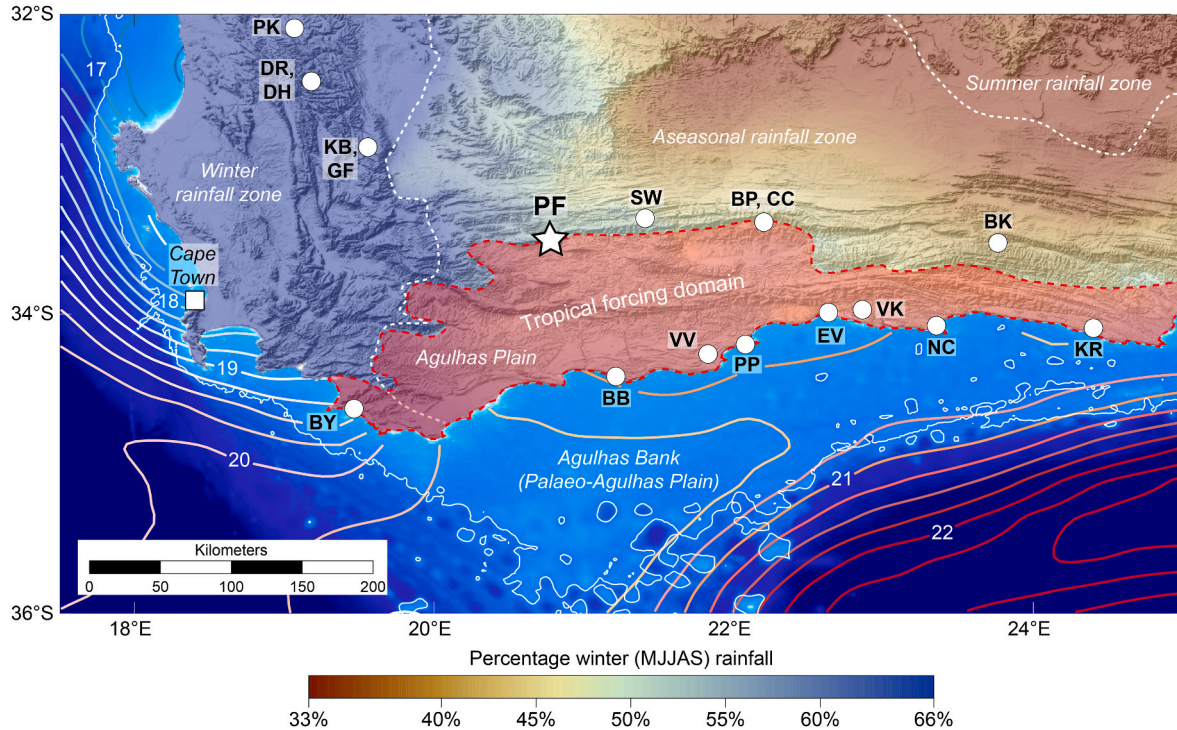


**Fig. 9.** Map of southern Cape study region and potential zone of tropical dominance. The location of the Papkuilfontein hyrax midden site (PF) is indicated, as are other key Holocene sites, including PK: Pakhuis Pass (Chase et al., 2019a; Scott and Woodborne, 2007a, 2007b), DR: De Rif (Chase et al., 2011, 2015a; Quick et al., 2011; Valsecchi et al., 2013), DH: Driehoek Vlei (Meadows and Sugden, 1991), KB: Katbakkies Pass (Chase et al., 2015b; Meadows et al., 2010), GF: Groenfontein (Chase et al., 2023), SW: Seweweekspruit (Chase et al., 2013, 2017), CC: Cango Caves (Chase et al., 2021; Talma and Vogel, 1992), VV: Voëlvlei (Strobel et al., 2021), EV: Eilandvlei (Quick et al., 2018; Wündsch et al., 2018), VK: Vankervelsvlei (Strobel et al., 2022), BK: Baviaanskloof (Chase et al., 2020) and the archaeological sites of BP: Boomplaas Cave (Deacon et al., 1984; Faith et al., 2018), BY: Byneskranskop (Faith et al., 2018; Schweitzer and Wilson, 1983), BB: Blombos Cave (Henshilwood et al., 2001), PP: Pinnacle Point (Marean, 2010), NC: Nelson Bay Cave (Deacon, 1978; Faith et al., 2018; Sealy et al., 2020) and KR: Klasies River Mouth (Deacon et al., 1986; Klein, 1975; Reynard and Wurz, 2020). Shading indicates the regional rainfall seasonality gradient defined according to Chase and Meadows (2007; data from Hijmans et al., 2005)), with winter, aseasonal and summer rainfall zones delimited by dashed white lines. The expanded extent of the zone of proposed tropical forcing domain is indicated by the dashed red line. The digital elevation model is from Yamazaki et al. (2017), the -130 m bathymetric isoline indicating the maximum extent of the Agulhas Plain during the Last Glacial Maximum is shown as a solid white line (data from GEBCO, 2012) and isolines indicating mean January sea-surfaces temperatures (1982–2010) at 0.25 °C intervals (data from Reynolds et al., 2007).

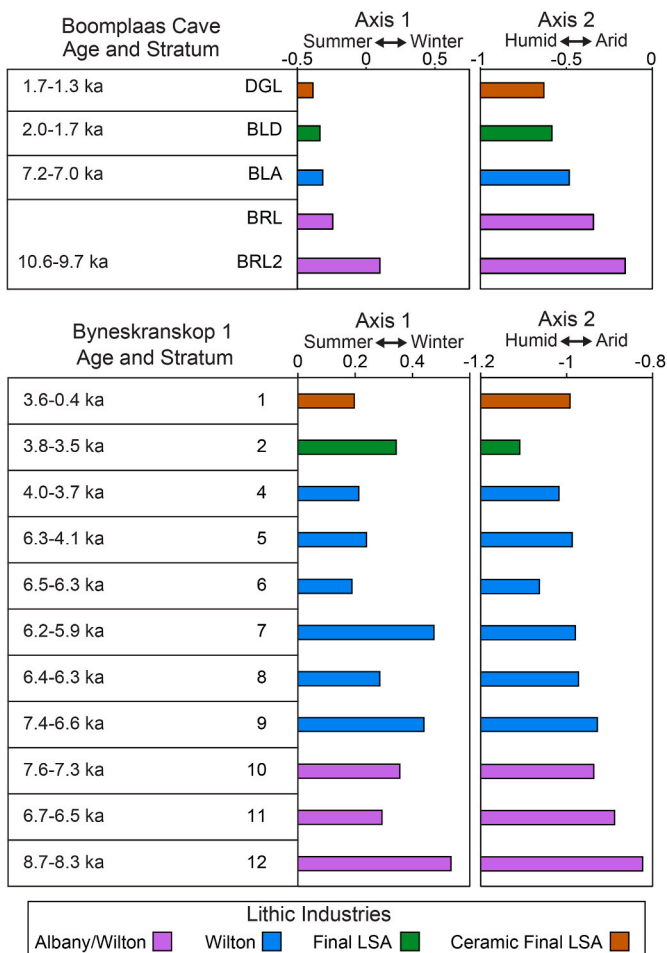


**Fig. 10.** Aridity and rainfall seasonality reconstructions from canonical correspondence analysis of microfaunal data from Boomplaas and Byneskranskop (Faith et al., 2018).

#### Declaration of competing interest

The authors declare that they have no known competing financial interests or personal relationships that could have appeared to influence the work reported in this paper.

#### Acknowledgements

The research leading to these results has received funding from the European Research Council under the European Union's Seventh Framework Programme (FP7/2007–2013), ERC Starting Grant "HYRAX", grant agreement no. 258657.

#### References

- Aranibar, J.N., Anderson, I.C., Epstein, H.E., Feral, C.J.W., Swap, R.J., Ramontsho, J., Macko, S.A., 2008. Nitrogen isotope composition of soils, C<sub>3</sub> and C<sub>4</sub> plants along land use gradients in southern Africa. *J. Arid Environ.* 72, 326–337.
- Austin, A.T., Vitousek, P.M., 1998. Nutrient dynamics on a precipitation gradient in Hawai'i. *Oecologia* 113, 519–529.
- Baker, A., Routh, J., Blaauw, M., Roychoudhury, A.N., 2014. Geochemical records of palaeoenvironmental controls on peat forming processes in the Mfabantzi peatland, KwaZulu Natal, South Africa since the late Pleistocene. *Palaeogeogr. Palaeoclimatol. Palaeoecol.* 395, 95–106.
- Bergh, N.G., Verboom, G.A., Rouget, M., Cowling, R.M., 2014. Vegetation types of the greater Cape Floristic region. In: Allsopp, N., Colville, J.F., Verboom, G.A. (Eds.), *Fynbos: Ecology, Evolution, and Conservation of a Megadiverse Region*. Oxford University Press, Oxford.
- Blaauw, M., Christen, J.A., 2011. Flexible paleoclimate age-depth models using an autoregressive gamma process. *Bayesian Analysis* 6, 457–474.
- Blaauw, M., Christen, J.A., A M L A, 2020. rbacon: Age-Depth Modelling using Bayesian Statistics. R package version 2.5.6.
- Braun, K., Bar-Matthews, M., Matthews, A., Ayalon, A., Zilberman, T., Cowling, R.M., Fisher, E.C., Herries, A.I.R., Brink, J.S., Marean, C.W., 2020. Comparison of climate and environment on the edge of the palaeo-Agulhas plain to the Little Karoo (South Africa) in marine isotope Stages 5–3 as indicated by speleothems. *Quat. Sci. Rev.* 235, 105803.
- Carr, A.S., Chase, B.M., Boom, A., Medina-Sánchez, J., 2016. Stable isotope analyses of rock hyrax faecal pellets, hyraceum and associated vegetation in southern Africa: implications for dietary ecology and palaeoenvironmental reconstructions. *J. Arid Environ.* 134, 33–48.
- Chase, B.M., 2021. Orbital forcing in southern Africa: towards a conceptual model for predicting deep time environmental change from an incomplete proxy record. *Quat. Sci. Rev.* 265, 107050.
- Chase, B.M., Boom, A., Carr, A.S., Carré, M., Chevalier, M., Meadows, M.E., Pedro, J.B., Stager, J.C., Reimer, P.J., 2015a. Evolving southwest African response to abrupt deglacial North Atlantic climate change events. *Quat. Sci. Rev.* 121, 132–136.
- Chase, B.M., Boom, A., Carr, A.S., Chevalier, M., Quick, L.J., Verboom, G.A., Reimer, P.J., 2019a. Extreme hydroclimate response gradients within the western Cape Floristic region of South Africa since the last glacial maximum. *Quat. Sci. Rev.* 219, 297–307.
- Chase, B.M., Boom, A., Carr, A.S., Meadows, M.E., Reimer, P.J., 2013. Holocene climate change in southernmost South Africa: rock hyrax middens record shifts in the southern westerlies. *Quat. Sci. Rev.* 82, 199–205.
- Chase, B.M., Boom, A., Carr, A.S., Quick, L.J., Reimer, P.J., 2020. High-resolution record of Holocene climate change dynamics from southern Africa's temperate-tropical boundary, Baviaanskloof, South Africa. *Palaeogeogr. Palaeoclimatol. Palaeoecol.* 539, 109518.
- Chase, B.M., Boom, A., Carr, A.S., Reimer, P.J., 2022. Climate variability along the margin of the southern African monsoon region at the end of the African Humid Period. *Quat. Sci. Rev.* 291, 107663.
- Chase, B.M., Carr, A.S., Boom, A., Tyrrell, G., Reimer, P.J., 2023. Linking upwelling intensity and orbital-scale climate variability in South Africa's winter rainfall zone: insights from a ~70,000-year hyrax midden record. *Quaternary Science Advances* 12, 100110.
- Chase, B.M., Carr, A.S., Boom, A., Tyrrell, G., Reimer, P.J., 2023. Linking upwelling intensity and orbital-scale climate variability in South Africa's winter rainfall zone: Insights from a ~70,000-year hyrax midden record. *Quaternary Science Advances* 12, 100110.
- Chase, B.M., Chevalier, M., Boom, A., Carr, A.S., 2017. The dynamic relationship between temperate and tropical circulation systems across South Africa since the last glacial maximum. *Quat. Sci. Rev.* 174, 54–62.
- Chase, B.M., Harris, C., de Wit, M.J., Kramers, J., Doel, S., Stankiewicz, J., 2021. South African Speleothems Reveal Influence of High- and Lowlatitude Forcing over the Past 113.5 k.y. *Geology*.
- Chase, B.M., Lim, S., Chevalier, M., Boom, A., Carr, A.S., Meadows, M.E., Reimer, P.J., 2015b. Influence of tropical easterlies in southern Africa's winter rainfall zone during the Holocene. *Quat. Sci. Rev.* 107, 138–148.
- Chase, B.M., Meadows, M.E., 2007. Late Quaternary dynamics of southern Africa's winter rainfall zone. *Earth Sci. Rev.* 84, 103–138.
- Chase, B.M., Meadows, M.E., Scott, L., Thomas, D.S.G., Marais, E., Sealy, J., Reimer, P.J., 2009. A record of rapid Holocene climate change preserved in hyrax middens from southwestern Africa. *Geology* 37, 703–706.
- Chase, B.M., Niedermeyer, E.M., Boom, A., Carr, A.S., Chevalier, M., He, F., Meadows, M. E., Ogle, N., Reimer, P.J., 2019b. Orbital controls on Namib Desert hydroclimate over the past 50,000 years. *Geology* 47, 867–871.
- Chase, B.M., Quick, L.J., 2018. Influence of Agulhas forcing of Holocene climate change in South Africa's southern Cape. *Quat. Res.* 90, 303–309.
- Chase, B.M., Quick, L.J., Meadows, M.E., Scott, L., Thomas, D.S.G., Reimer, P.J., 2011. Late glacial interhemispheric climate dynamics revealed in South African hyrax middens. *Geology* 39, 19–22.
- Chase, B.M., Scott, L., Meadows, M.E., Gil-Romera, G., Boom, A., Carr, A.S., Reimer, P.J., Truc, L., Valsecchi, V., Quick, L.J., 2012. Rock hyrax middens: a palaeoenvironmental archive for southern African drylands. *Quat. Sci. Rev.* 56, 107–125.
- Chevalier, M., Chase, B.M., 2015. Southeast African records reveal a coherent shift from high- to low-latitude forcing mechanisms along the east African margin across last glacial-interglacial transition. *Quat. Sci. Rev.* 125, 117–130.
- Cockcroft, M.J., Wilkinson, M.J., Tyson, P.D., 1987. The application of a present-day climatic model to the late Quaternary in southern Africa. *Climatic Change* 10, 161–181.
- Cooper, G.R.J., Cowan, D.R., 2008. Comparing time series using wavelet-based semblance analysis. *Comput. Geosci.* 34, 95–102.
- Cowling, R.M., Lombard, A.T., 2002. Heterogeneity, speciation/extinction history and climate: explaining regional plant diversity patterns in the Cape Floristic Region. *Divers. Distrib.* 8, 163–179.
- Craine, J.M., Elmore, A.J., Aidar, M.P.M., Bustamante, M., Dawson, T.E., Hobbie, E.A., Kahmen, A., Mack, M.C., McLauchlan, K.K., Michelsen, A., Nardoto, G.B., Pardo, L. H., Peñuelas, J., Reich, P.B., Schuur, E.A.G., Stock, W.D., Templar, P.H., Virginia, R. A., Welker, J.M., Wright, I.J., 2009. Global patterns of foliar nitrogen isotopes and their relationships with climate, mycorrhizal fungi, foliar nutrient concentrations, and nitrogen availability. *New Phytol.* 183, 980–992.
- Dansgaard, W., 1964. Stable isotopes in precipitation. *Tellus* 16, 436–447.
- David, J.N., 2017. Changes in Precipitation over Southern Africa during Recent Centuries.

- Deacon, H.J., Deacon, J., Scholtz, A., Thackeray, J.F., Brink, J.S., 1984. Correlation of palaeoenvironmental data from the late Pleistocene and Holocene deposits at Boomplaas cave, southern Cape. In: Vogel, J.C. (Ed.), Late Cainozoic Palaeoclimates of the Southern Hemisphere. Balkema, Rotterdam, pp. 339–360.
- Deacon, H.J., Geleijnse, V.B., Thackeray, A.I., Thackeray, J.F., Tusenius, M.L., Vogel, J. C., 1986. Late Pleistocene cave deposits in the southern Cape: current research at Klasies River. In: Proc. 7th SASQUA Conference. Palaeoecology of Africa, vol. 17, pp. 31–37. Stellenbosch, 1985.
- Deacon, J., 1978. Changing patterns in the late Pleistocene/early Holocene prehistory of southern Africa as seen from the Nelson Bay cave Stone artifact sequence. *Quat. Res.* 10, 84–111.
- Deacon, J., Lancaster, N., 1988. Late Quaternary Palaeoenvironments of Southern Africa. Clarendon Press, Oxford.
- Engelbrecht, C.J., Landman, W.A., 2016. Interannual variability of seasonal rainfall over the Cape south coast of South Africa and synoptic type association. *Clim. Dynam.* 47, 295–313.
- Faith, J.T., 2013. Taphonomic and paleoecological change in the large mammal sequence from Boomplaas Cave, Western Cape, South Africa. *J. Hum. Evol.* 65, 715–730.
- Faith, J.T., Chase, B.M., Avery, D.M., 2018. Late Quaternary micromammals and the precipitation history of the southern Cape, South Africa. *Quat. Res.* 91, 848–860.
- Faith, J.T., Chase, B.M., Pargeter, J., 2023. The last glacial maximum climate at Boomplaas cave, South Africa. *Quat. Sci. Rev.*
- Finch, J.M., Hill, T.R., 2008. A late Quaternary pollen sequence from Mfabeni Peatland, South Africa: Reconstructing forest history in Maputaland. *Quat. Res.* 70, 442–450.
- GEOBCO, 2012. The GEOBCO\_08 Grid version 20120320.
- Hammer, Ø., Harper, D.A.T., Ryan, P.D., 2001. PAST: Paleontological Statistics software package for Education and data analysis. *Paleaeontol. Electron.* 4, 9.
- Handley, L.L., Austin, A.T., Stewart, G.R., Robinson, D., Scrimgeour, C.M., Raven, J.A., Heaton, T.H.E., Schmidt, S., 1999. The  $\delta^{15}\text{N}$  natural abundance ( $\delta^{15}\text{N}$ ) of ecosystem samples reflects measures of water availability. *Funct. Plant Biol.* 26, 185–199.
- Harris, C., Burgers, C., Miller, J., Rawoot, F., 2010. O- and H-isotope record of Cape Town rainfall from 1996 to 2008, and its application to recharge studies of Table Mountain groundwater, South Africa. *S. Afr. J. Geol.* 113, 33–56.
- Hart, N.C.G., Washington, R., Reason, C.J.C., 2018. On the Likelihood of tropical-Extratropical Cloud bands in the South Indian Convergence zone during ENSO events. *J. Clim.* 31, 2797–2817.
- Hartman, G., 2011. Are elevated  $\delta^{15}\text{N}$  values in herbivores in hot and arid environments caused by diet or animal physiology? *Funct. Ecol.* 25, 122–131.
- Hartman, G., Danin, A., 2010. Isotopic values of plants in relation to water availability in the Eastern Mediterranean region. *Oecologia* 162, 837–852.
- Henshilwood, C.S., d'Errico, F., Marean, C.W., Milo, R.G., Yates, R., 2001. An early bone tool industry from the Middle Stone Age at Blombos Cave, South Africa: implications for the origins of modern human behaviour, symbolism and language. *J. Hum. Evol.* 41, 631–678.
- Hijmans, R., Cameron, S.E., Parra, J.L., Jones, P.G., Jarvis, A., 2005. Very high resolution interpolated climate surfaces for global land areas. *Int. J. Climatol.* 25, 1965–1978.
- Hogg, A.G., Heaton, T.J., Hua, Q., Palmer, J.G., Turney, C.S.M., Souton, J., Bayliss, A., Blackwell, P.G., Boswijk, G., Bronk Ramsey, C., Pearson, C., Petchey, F., Reimer, P., Reimer, R., Wacker, L., 2020. SHCal20 southern Hemisphere calibration, 0–55,000 years cal BP. *Radiocarbon* 1–20.
- Holmgren, K., Lee-Thorp, J.A., Cooper, G.R.J., Lundblad, K., Partridge, T.C., Scott, L., Sithaldeen, R., Siep Talma, A., Tyson, P.D., 2003. Persistent millennial-scale climatic variability over the past 25,000 years in Southern Africa. *Quat. Sci. Rev.* 22, 2311–2326.
- Hua, Q., Turnbull, J.C., Santos, G.M., Rakowski, A.Z., Ancapichún, S., De Pol-Holz, R., Hammer, S., Lehman, S.J., Levin, I., Miller, J.B., Palmer, J.G., Turney, C.S.M., 2021. Atmospheric radiocarbon for the period 1950–2019. *Radiocarbon* 1–23.
- Killick, R., Fearnhead, P., Eckley, I.A., 2012. Optimal detection of Changepoints with a linear Computational Cost. *J. Am. Stat. Assoc.* 107, 1590–1598.
- Klein, R.G., 1972. The late Quaternary mammalian fauna of Nelson Bay Cave (Cape Province, South Africa): its implications for megafaunal extinctions and environmental and cultural change. *Quat. Res.* 2, 135–142.
- Klein, R.G., 1975. Middle Stone age Man-animal relationships in southern Africa: evidence from Die Kelders and Klasies River Mouth. *Science* 190, 265–267.
- Landman, W.A., Beraki, A., 2012. Multi-model forecast skill for mid-summer rainfall over southern Africa. *Int. J. Climatol.* 32, 303–314.
- Laskar, J., Robutel, P., Joutel, F., Gastineau, M., Correia, A.C.M., Levrard, B., 2004. A long-term numerical solution for the insolation quantities of the Earth. *A&A* 428, 261–285.
- Lee-Thorp, J.A., Holmgren, K., Lauritzen, S.-E., Linge, H., Moberg, A., Partridge, T.C., Stevenson, C., Tyson, P.D., 2001. Rapid climate shifts in the southern African interior throughout the mid- to late Holocene. *Geophys. Res. Lett.* 28, 4507–4510.
- Loftus, E., Sealy, J., Lee-Thorp, J., 2016. New radiocarbon dates and Bayesian models for Nelson Bay cave and Byneskranskop 1: implications for the South African later Stone age sequence. *Radiocarbon FirstView* 1–17.
- Marean, C.W., 2010. Pinnacle point cave 13B (western Cape Province, South Africa) in context: the Cape Floral kingdom, shellfish, and modern human origins. *J. Hum. Evol.* 59, 425–443.
- Martin, A.R.H., 1968. Pollen analysis of Groenvlei lake sediments, Knysna (South Africa). *Rev. Palaeobot. Palynol.* 7, 107–144.
- Meadows, M.E., Chase, B.M., Seliane, M., 2010. Holocene palaeoenvironments of the Cederberg and Swartruggens mountains, Western Cape, South Africa: pollen and stable isotope evidence from hyrax dung middens. *J. Arid Environ.* 74, 786–793.
- Meadows, M.E., Sugden, J.M., 1991. A vegetation history of the last 14,000 years on the Cederberg, southwestern Cape Province. *South Afr. J. Sci.* 87, 34–43.
- Metwally, A.A., Scott, L., Neumann, F.H., Bamford, M.K., Oberhänsli, H., 2014. Holocene palynology and palaeoenvironments in the Savanna biome at Tswaing Crater, central South Africa. *Palaeogeogr. Palaeoclimatol. Palaeoecol.* 402, 125–135.
- Mucina, L., Jürgens, N., Le Roux, A., Rutherford, M.C., Schmiedel, U., Esler, K.J., Powrie, L.W., Desmet, P.G., Milton, S.J., 2006. Succulent Karoo biome. In: Mucina, L., Rutherford, M.C. (Eds.), *The Vegetation of South Africa, Lesotho and Swaziland*. South African National Biodiversity Institute, Pretoria, pp. 221–299.
- Murphy, B.P., Bowman, D.M.J.S., 2006. Kangaroo metabolism does not cause the relationship between bone collagen  $\delta^{15}\text{N}$  and water availability. *Funct. Ecol.* 20, 1062–1069.
- Murphy, B.P., Bowman, D.M.J.S., 2009. The carbon and nitrogen isotope composition of Australian grasses in relation to climate. *Funct. Ecol.* 23, 1040–1049.
- Neumann, F.H., Scott, L., Bousman, C.B., van As, L., 2010. A Holocene sequence of vegetation change at Lake Eteza, coastal KwaZulu-Natal, South Africa. *Rev. Palaeobot. Palynol.* 162, 39–53.
- Newsome, S.D., Miller, G.H., Magee, J.W., Fogel, M.L., 2011. Quaternary record of aridity and mean annual precipitation based on  $\delta^{15}\text{N}$  in ratite and dromornithid eggshells from Lake Eyre, Australia. *Oecologia* 167, 1151–1162.
- Nicholson, S.E., Kim, J., 1997. The relationship of El Niño-southern oscillation to African rainfall. *Int. J. Climatol.* 17, 117–135.
- Nielsen, S.H.H., Koç, N., Crosta, X., 2004. Holocene climate in the Atlantic sector of the Southern Ocean: controlled by insolation or oceanic circulation? *Geology* 32, 317–320.
- Norström, E., Scott, L., Partridge, T.C., Risberg, J., Holmgren, K., 2009. Reconstruction of environmental and climate changes at Braamhoek wetland, eastern escarpment South Africa, during the last 16,000 years with emphasis on the Pleistocene-Holocene transition. *Palaeogeogr. Palaeoclimatol. Palaeoecol.* 271, 240–258.
- Pargeter, J., Loftus, E., Mackay, A., Mitchell, P., Stewart, B., 2018. New ages from Boomplaas Cave, South Africa, provide increased resolution on late/terminal Pleistocene human behavioural variability. *Azania* 53, 156–184.
- Partridge, T.C., deMenocal, P.B., Lorentz, S.A., Paikar, M.J., Vogel, J.C., 1997. Orbital forcing of climate over South Africa: a 200,000-year rainfall record from the Pretoria Saltpan. *Quat. Sci. Rev.* 16, 1125–1133.
- Peel, M.C., Finlayson, B.L., McMahon, T.A., 2007. Updated world map of the Köppen-Geiger climate classification. *Hydrol. Earth Syst. Sci.* 11, 1633–1644.
- Quick, L.J., Carr, A.S., Meadows, M.E., Boom, A., Bateman, M.D., Roberts, D.L., Reimer, P.J., Chase, B.M., 2015. A late Pleistocene-Holocene multi-proxy record of palaeoenvironmental change from Still Bay, southern Cape Coast, South Africa. *J. Quat. Sci.* 30, 870–885.
- Quick, L.J., Chase, B.M., Carr, A.S., Chevalier, M., Grobler, B.A., Meadows, M.E., 2021. A 25,000 year record of climate and vegetation change from the southwestern Cape coast, South Africa. *Quat. Res.* 105, 82–99.
- Quick, L.J., Chase, B.M., Meadows, M.E., Scott, L., Reimer, P.J., 2011. A 19.5 kyr vegetation history from the central Cederberg Mountains, South Africa: palynological evidence from rock hyrax middens. *Palaeogeogr. Palaeoclimatol. Palaeoecol.* 309, 253–270.
- Quick, L.J., Chase, B.M., Wündsch, M., Kirsten, K.L., Chevalier, M., Mäusbacher, R., Meadows, M.E., Haberzettl, T., 2018. A high-resolution record of Holocene climate and vegetation dynamics from the southern Cape coast of South Africa: pollen and microcharcoal evidence from Eilandleie. *J. Quat. Sci.* 33, 487–500.
- Quick, L.J., Meadows, M.E., Bateman, M.D., Kirsten, K.L., Mäusbacher, R., Haberzettl, T., Chase, B.M., 2016. Vegetation and climate dynamics during the last glacial period in the fynbos-afrotropical forest ecotone, southern Cape, South Africa. *Quat. Int.* 404 (Part B), 136–149.
- Reason, C.J.C., Allan, R.J., Lindesay, J.A., Ansell, T.J., 2000. ENSO and climatic signals across the Indian Ocean basin in the global context: Part I, interannual composite patterns. *Int. J. Climatol.* 20, 1285–1327.
- Rebelo, A.G., Boucher, C., Helme, N., Mucina, L., Rutherford, M.C., 2006. Fynbos biome. In: Mucina, L., Rutherford, M.C. (Eds.), *The Vegetation of South Africa, Lesotho and Swaziland*. South African National Biodiversity Institute, Pretoria, pp. 53–219.
- Rehfeld, K., Marwan, N., Heitzig, J., Kurths, J., 2011. Comparison of correlation analysis techniques for irregularly sampled time series. *Nonlinear Process Geophys.* 18, 389–404.
- Reimer, R.W., Reimer, P.J., 2023. CALIBomb, 2023-04-05.
- Rein, B., Lückge, A., Reinhardt, L., Sirocko, F., Wolf, A., Dullo, W.-C., 2005. El Niño variability off Peru during the last 20,000 years. *Paleoceanography* 20.
- Reynard, J.P., Wurz, S., 2020. The palaeoecology of Klasies River, South Africa: an analysis of the large mammal remains from the 1984–1995 excavations of Cave 1 and 1A. *Quat. Sci. Rev.* 237, 106301.
- Reynolds, R.W., Smith, T.M., Liu, C., Chelton, D.B., Casey, K.S., Schlax, M.G., 2007. Daily high-resolution-blended analyses for sea surface temperature. *J. Clim.* 20, 5473–5496.
- Rouault, M., White, S.A., Reason, C.J.C., Lutjeharms, J.R.E., Jobard, I., 2002. Ocean–Atmosphere interaction in the Agulhas current region and a South African extreme weather event. *Weather Forecast.* 17, 655.
- Schefuß, E., Kuhlmann, H., Mollenhauer, G., Prange, M., Pätzold, J., 2011. Forcing of wet phases in southeast Africa over the past 17,000 years. *Nature* 480, 509–512.
- Schweitzer, F.R., Wilson, M.L., 1983. Byneskranskop 1: A Late Quaternary Living Site in the Southern Cape Province, South Africa. The Rustica Press, Cape Town.
- Scott, L., 1982. A late Quaternary pollen record from the Transvaal bushveld, South Africa. *Quat. Res.* 17, 339–370.
- Scott, L., 1987a. Late quaternary forest history in Venda, southern Africa. *Rev. Palaeobot. Palynol.* 53, 1–10.
- Scott, L., 1987b. Pollen analysis of hyena coprolites and sediments from Equus Cave, Taung, southern Kalahari (South Africa). *Quat. Res.* 28, 144–156.

- Scott, L., 1999. Vegetation history and climate in the Savanna biome South Africa since 190,000 ka: a comparison of pollen data from the Tswaing Crater (the Pretoria Saltpan) and Wonderkrater. *Quat. Int.* 57–8, 215–223.
- Scott, L., Bousman, C.B., Nyakale, M., 2005. Holocene pollen from swamp, cave and hyrax dung deposits at Blydefontein (Kikvorsberge), Karoo, South Africa. *Quat. Int.* 129, 49–59.
- Scott, L., Neumann, F.H., Brook, G.A., Bousman, C.B., Norström, E., Metwally, A.A., 2012. Terrestrial fossil-pollen evidence of climate change during the last 26 thousand years in southern Africa. *Quat. Sci. Rev.* 32, 100–118.
- Scott, L., Nyakale, M., 2002. Pollen indications of Holocene palaeoenvironments at Florisbad spring in the central free state, South Africa. *Holocene* 12, 497–503.
- Scott, L., Vogel, J.C., 1983. Late quaternary pollen profile from the transvaal highveld, South Africa. *South Afr. J. Sci.* 79, 266–272.
- Scott, L., Woodborne, S., 2007a. Pollen analysis and dating of late quaternary faecal deposits (hyraceum) in the cederberg, western Cape, South Africa. *Rev. Palaeobot. Palynol.* 144, 123–134.
- Scott, L., Woodborne, S., 2007b. Vegetation history inferred from pollen in Late Quaternary faecal deposits (hyraceum) in the Cape winter-rain region and its bearing on past climates in South Africa. *Quat. Sci. Rev.* 26, 941–953.
- Sealy, J., 1996. Seasonality of rainfall around the Last Glacial Maximum as reconstructed from carbon isotope analyses of animal bones from Nelson Bay Cave. *South Afr. J. Sci.* 92, 441–444.
- Sealy, J., Lee-Thorp, J., Loftus, E., Faith, J.T., Marean, C.W., 2016. Late Quaternary environmental change in the Southern Cape, South Africa, from stable carbon and oxygen isotopes in faunal tooth enamel from Boomplaas Cave. *J. Quat. Sci.* 31, 919–927.
- Sealy, J., Naidoo, N., Hare, V.J., Brunton, S., Faith, J.T., 2020. Climate and ecology of the palaeo-Agulhas Plain from stable carbon and oxygen isotopes in bovid tooth enamel from Nelson Bay Cave, South Africa. *Quat. Sci. Rev.* 235, 105974.
- Slota, P.J., Jull, A.J.T., Linick, T.W., Toolin, L.J., 1987. Preparation of small samples for  $^{14}\text{C}$  accelerator targets by catalytic reduction of CO. *Radiocarbon* 29, 303–306.
- Strobel, P., Bliedtner, M., Carr, A.S., Frenzel, P., Klaes, B., Salazar, G., Struck, J., Szidat, S., Zech, R., Haberzettl, T., 2021. Holocene sea level and environmental change at the southern Cape – an 8.5 kyr multi-proxy paleoclimate record from Lake Voëlvlei, South Africa. *Clim. Past* 17, 1567–1586.
- Strobel, P., Bliedtner, M., Carr, A.S., Struck, J., du Plessis, N., Glaser, B., Meadows, M.E., Quick, L.J., Zech, M., Zech, R., Haberzettl, T., 2022. Reconstructing Late Quaternary precipitation and its source on the southern Cape coast of South Africa: a multi-proxy paleoenvironmental record from Vankervelsvlei. *Quat. Sci. Rev.* 284, 107467.
- Strobel, P., Henning, T., Bliedtner, M., Mosher, S.G., Rahimova, H., Haberzettl, T., Kirsten, K.L., Lehndorff, E., Power, M.J., Zech, M., Zech, R., 2024. Holocene fire dynamics and their climatic controls on the southern Cape coast of South Africa - a 7.2 ka multi-proxy record from the peatland Vankervelsvlei. *Quat. Sci. Rev.* 325, 108464.
- Swap, R.J., Aranibar, J.N., Dowty, P.R., Gilhooly, W.P., Macko, S.A., 2004. Natural abundance of  $^{13}\text{C}$  and  $^{15}\text{N}$  in  $\text{C}_3$  and  $\text{C}_4$  vegetation of southern Africa: patterns and implications. *Global Change Biol.* 10, 350–358.
- Talma, A.S., Vogel, J.C., 1992. Late quaternary paleotemperatures derived from a speleothem from Cango Caves, Cape province, South Africa. *Quat. Res.* 37, 203–213.
- Tozuka, T., Abiodun, B.J., Engelbrecht, F.A., 2014. Impacts of convection schemes on simulating tropical-temperate troughs over southern Africa. *Clim. Dynam.* 42, 433–451.
- Valsecchi, V., Chase, B.M., Slingsby, J.A., Carr, A.S., Quick, L.J., Meadows, M.E., Cheddadi, R., Reimer, P.J., 2013. A high resolution 15,600-year pollen and microcharcoal record from the Cederberg Mountains, South Africa. *Palaeogeogr. Palaeoclimatol. Palaeoecol.* 387, 6–16.
- van Zinderen Bakker, E.M., 1976. The evolution of late Quaternary paleoclimates of Southern Africa. *Palaeoecol. Afr.* 9, 160–202.
- Weldon, D., Reason, C.J.C., 2014. Variability of rainfall characteristics over the South Coast region of South Africa. *Theor. Appl. Climatol.* 115, 177–185.
- Wündsch, M., Haberzettl, T., Cawthra, H.C., Kirsten, K.L., Quick, L.J., Zabel, M., Frenzel, P., Hahn, A., Baade, J., Daut, G., Kasper, T., Meadows, M.E., Mäusbacher, R., 2018. Holocene environmental change along the southern Cape coast of South Africa – insights from the Eilandvlei sediment record spanning the last 8.9 kyr. *Global Planet. Change* 163, 51–66.
- Yamazaki, D., Ikeshima, D., Tawatari, R., Yamaguchi, T., O'Loughlin, F., Neal, J.C., Sampson, C.C., Kanae, S., Bates, P.D., 2017. A high-accuracy map of global terrain elevations. *Geophys. Res. Lett.* 44, 5844–5853.
- Zeileis, A., Grothendieck, G., 2005. Zoo: S3 infrastructure for regular and irregular time series. *J. Stat. Software* 14, 1–27.
- Zinke, J., Dullo, W.C., Heiss, G.A., Eisenhauer, A., 2004. ENSO and Indian Ocean subtropical dipole variability is recorded in a coral record off southwest Madagascar for the period 1659 to 1995. *Earth Planet. Sci. Lett.* 228, 177–194.